# Dark Light-Higgs Bosons

Patrick Draper,[1] Tao Liu,[1,2] Carlos E. M. Wagner,[1,3,4] Lian-Tao Wang,[5] and Hao Zhang[1,6]
[1]*Enrico Fermi Institute, University of Chicago, Chicago, Illinois 60637, USA*
[2]*Department of Physics, University of California, Santa Barbara, California 93106, USA*
[3]*HEP Division, Argonne National Laboratory, 9700 Cass Avenue, Argonne, Illinois 60439, USA*
[4]*KICP and Department of Physics, University of Chicago, 5640 South Ellis Avenue, Chicago Illinois 60637, USA*
[5]*Department of Physics, Princeton University, Princeton, New Jersey 08540, USA*
[6]*Department of Physics and State Key Laboratory of Nuclear Physics and Technology, Peking University, Beijing 100871, China*
(Received 14 October 2010; published 24 March 2011)

We study a limit of the nearly Peccei-Quinn-symmetric next-to-minimal supersymmetric standard model possessing novel Higgs and dark matter (DM) properties. In this scenario, there naturally coexist three light singletlike particles: a scalar, a pseudoscalar, and a singlinolike DM candidate, all with masses of order 0.1–10 GeV. The decay of a standard model-like Higgs boson to pairs of the light scalars or pseudoscalars is generically suppressed, avoiding constraints from collider searches for these channels. For a certain parameter window annihilation into the light pseudoscalar and exchange of the light scalar with nucleons allow the singlino to achieve the correct relic density and a large direct-detection cross section consistent with the DM direct-detection experiments, CoGeNT and DAMA/LIBRA, preferred region simultaneously. This parameter space is consistent with experimental constraints from LEP, the Tevatron, $\Upsilon$, and flavor physics.

DOI: 10.1103/PhysRevLett.106.121805 PACS numbers: 14.80.Da, 12.60.Jv, 95.35.+d

The next-to-minimal supersymmetric standard model (NMSSM) is a well-motivated extension of the minimal supersymmetric standard model (MSSM) by a gauge-singlet chiral superfield $\mathbf{N}$, designed to solve the $\mu$ problem of the MSSM. Its superpotential and soft supersymmetry-breaking terms in the Higgs sector are

$$\mathbf{W} = \lambda \mathbf{N}\mathbf{H_u}\mathbf{H_d} + \frac{1}{3}\kappa \mathbf{N}^3,$$
$$V_{\rm soft} = m_{H_d}^2|H_d|^2 + m_{H_u}^2|H_u|^2 + m_N^2|N|^2 - (\lambda A_\lambda H_u H_d N + \text{H.c.}) + \left(\frac{\kappa}{3}A_\kappa N^3 + \text{H.c.}\right). \quad (1)$$

Here $H_d$, $H_u$, and $N$ denote the neutral Higgs bosons corresponding to $\mathbf{H_d}$, $\mathbf{H_u}$, and $\mathbf{N}$, respectively.

In this work, we examine a NMSSM limit given by two conditions. The first one is $\kappa \ll \lambda$, which is protected by an approximate Peccei-Quinn (PQ) symmetry. A light pseudoscalar $a_1$ will be generated by the spontaneous breaking of such a $U(1)$ symmetry (the phenomenology on a light $a_1$ has been studied in the $R$-symmetry limit [1,2]). As noted in [3], at tree level the PQ limit implies an upper bound on the lightest scalar mass $m_{h_1}$ approximately proportional to $\lambda^2$. Here we address the further limit of $\lambda \lesssim 0.1$, leading to the simultaneous emergence of a light singletlike scalar $h_1$ and a light singlinolike lightest superpartner $\chi_1$. For mildly small values of $\lambda$ ($\lambda > 0.05$) studied in this Letter, typically $\lambda(\Lambda_{\rm GUT}) \sim \mathcal{O}(0.1)$, a natural order for a perturbative parameter. We stress that this scenario differs from the light $a_1$ case of [1,2], in that $h_1$, $a_1$, and $\chi_1$ are all of order 0.1–10 GeV. It also differs in that decays of the standard model (SM)-like Higgs boson to $h_1h_1$ and $a_1a_1$ pairs are generically suppressed. Thus, $h_1$ and $a_1$ are hidden from four-fermion searches at LEP [4] and the Tevatron [5] designed to test a light $a_1$ scenario. Meanwhile, due to annihilation into $a_1$ and exchange of $h_1$, for a certain window of the parameters, the correct relic density and a large spin-independent (SI) direct-detection cross section consistent with the CoGeNT and DAMA/LIBRA preferred region can be achieved for the dark matter (DM) candidate $\chi_1$. Therefore, we refer to this limit as the "dark light-Higgs" (DLH) scenario.

We begin with an analysis of the light spectrum in the DLH scenario. For convenience we define two parameters,

$$\varepsilon \equiv \frac{\lambda\mu}{m_Z}\varepsilon', \qquad \varepsilon' \equiv \frac{A_\lambda}{\mu\tan\beta} - 1, \quad (2)$$

with $\mu \equiv \lambda\langle N\rangle$. In the first column of Fig. 1 we plot $m_{h_1,a_1,\chi_1}$ against $\varepsilon$ for a random scan as defined in the caption. NMSSMTOOLS 2.3.1 and MICROMEGAS 2.4.Q [6,7] are our analysis tools used in this Letter.

The scan results in Fig. 1 can be understood analytically as follows. Because of the spontaneous breaking of the approximate PQ symmetry, $a_1$ is a pseudo-Goldstone boson and its small mass $m_{a_1}^2 \approx -3\kappa A_\kappa \mu/\lambda$ is protected. For $\chi_1$, $\kappa \ll \lambda \ll 1$ implies that it is dominantly singlino and its mass is $m_{\chi_1} \approx v^2\lambda^2 \sin 2\beta/\mu + 2\kappa\mu/\lambda$, where $v =$ 174 GeV and $\tan\beta \equiv \langle H_u\rangle/\langle H_d\rangle$. For $\lambda \lesssim 0.1$, $\mu$ of order a few hundred GeV, and $\kappa/\lambda$ on the order of a few percent, $m_{\chi_1}$ drops below 10 GeV.

More interesting is the $CP$-even spectrum. For analytic convenience we consider moderate $\tan\beta$, although the qualitative properties of the figures are also present for lower $\tan\beta$. In the small $\lambda$ + PQ limit, $h_1$ has a mass

 

$$(m_{h_1}^2)_{\rm tree} \approx -4v^2\varepsilon^2 + \frac{4v^2\lambda^2}{\tan^2\beta} + \frac{\kappa A_\kappa \mu}{\lambda} + \frac{4\kappa^2\mu^2}{\lambda^2} \quad (3)$$

at tree level. The heaviest state is strongly down type, with a mass $m_{h_3}^2 \simeq m_{H_d}^2 \simeq A_\lambda^2$ and the middle state is SM-like.

The $h_1$ mass is lifted by quantum corrections. The singletlike nature of $h_1$ suppresses contributions from all particles running in the loop except Higgs bosons and Higgsinos, which gives

$$\Delta m_{h_1}^2 \approx \frac{\lambda^2\mu^2}{2\pi^2}\log\frac{\mu^2\tan\beta^3}{m_Z^2}. \quad (4)$$

Fixing all other parameters, the upper bound on $m_{h_1}^2$ is achieved for $\varepsilon \to 0$ and is lowered to about or below 10 GeV in the small $\lambda$ + PQ limit.

On the other hand, increasing $\varepsilon$ rapidly decreases $m_{h_1}$. Vacuum stability [i.e., $(m_{h_1}^2)_{\rm tree} + \Delta m_{h_1}^2 \geq 0$] indicates

$$\varepsilon_{\rm max}^2 \approx \frac{1}{4v^2}\left(\frac{4\lambda^2 v^2}{\tan^2\beta} + \frac{\kappa A_\kappa \mu}{\lambda} + \frac{4\kappa^2\mu^2}{\lambda^2} + \Delta m_{h_1}^2\right). \quad (5)$$

In the small $\lambda$ + PQ limit and for natural values of $\mu$, $|\varepsilon_{\rm max}|$ is small. The bottom right-hand panel of Fig. 1 also shows

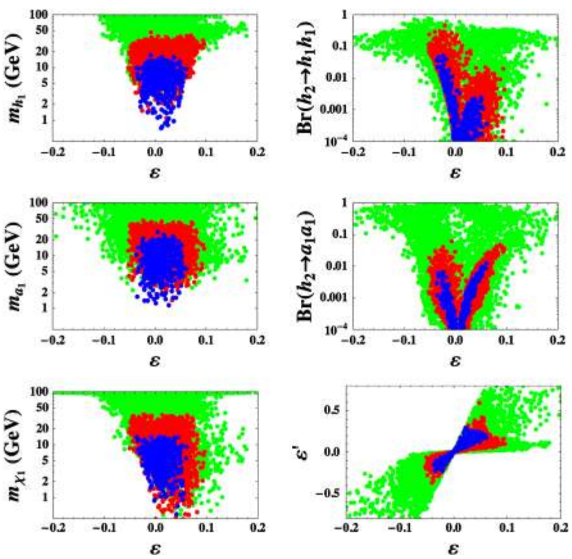

FIG. 1 (color online). Masses of $h_1$ (top left), $a_1$ (middle left), and $\chi_1$ (bottom left); branching ratios of $h_2$ into $h_1h_1$ (top right) and $a_1a_1$ (middle right), and correlation between $\varepsilon$ and $\varepsilon'$ (bottom right). Points are taken randomly from the ranges $5 \leq \tan\beta \leq 50$, $0.05 \leq \lambda \leq 0.5$, $0.0005 \leq \kappa \leq 0.05$, $-0.8 \leq \varepsilon' \leq 0.8$, $-40 \leq A_\kappa \leq 0$ GeV, and $0.1 \leq \mu \leq 1$ TeV. (As an illustration, we assume soft squark masses of 1 TeV, slepton masses of 200 GeV, $A_{u,d,e}$ parameters of 750 GeV, and bino, wino, and gluino masses of 100, 200, and 660 GeV, respectively, for all numerical analyses in this Letter.) Light gray (green) points cover the whole scan range, gray (red) points correspond to $\lambda < 0.30$, $\kappa/\lambda < 0.05$, and $\mu < 400$ GeV, and dark gray (blue) points correspond to $\lambda < 0.15$, $\kappa/\lambda < 0.03$, and $\mu < 250$ GeV.

that $A_\lambda$ is usually close to $\mu\tan\beta$ for blue points, so we will take a smaller range of $\epsilon'$ in our DM analysis.

The tree-level mixing parameters of the light scalar are

$$S_{1d} \approx \frac{v}{\mu\tan\beta}\left(\lambda + \frac{2\varepsilon\mu}{m_Z}\right), \qquad S_{1u} \approx \frac{2v\varepsilon}{m_Z}, \quad (6)$$

indicating a mostly singlet and down admixture in the limit $\varepsilon \to 0$ and an approximately pure singlet (i.e., $S_{1s} \to 1$) in the further limit of small $\lambda$ or large $\tan\beta$.

Similarly to the light $a_1$ scenario of [2], relevant constraints may come from the searches for [4,5]

$$h_2 \to h_1h_1,\, a_1a_1 \to 4b,\, 4\tau,\, 2b2\tau \quad \text{(LEP)},$$

$$h_2 \to h_1h_1,\, a_1a_1 \to 4\mu,\, 2\mu2\tau \quad \text{(Tevatron)}.$$

However, in our case the tree-level couplings of $h_2$ to $h_1h_1$ and $a_1a_1$ are suppressed. This can be seen as follows. Since $h_1$ is strongly singletlike and $h_2$ is up type, the coupling $y_{h_2h_1h_1}$ is (for a complete formula, see [8])

$$y_{h_2h_1h_1} \approx -\frac{\lambda v m_Z \varepsilon}{\sqrt{2}\mu}. \quad (7)$$

Here we use the mixing parameters at lowest order in $\varepsilon$,

$$S_{2d} \approx \cot\beta, \qquad S_{2s} \approx -\frac{2\varepsilon v m_Z}{m_Z^2 + \mu^2}, \quad (8)$$

for moderate $\tan\beta$. Similarly, one can find $y_{h_2a_1a_1} = y_{h_2h_1h_1}$ at this order. Both $\mathrm{Br}(h_2 \to h_1h_1)$ and $\mathrm{Br}(h_2 \to a_1a_1)$ are thus suppressed by $\lambda\varepsilon \ll 1$, as is shown in the right-hand column of Fig. 1. (Instead, $h_2$ can dominantly decay into $\chi_1$ and $\chi_2$, while $\chi_2$ dominantly decays into light-Higgs

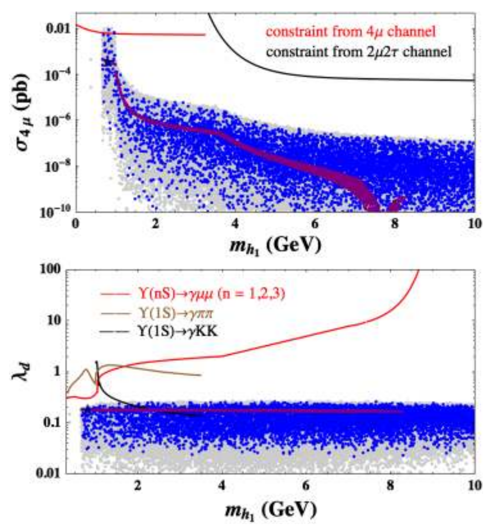


FIG. 2 (color online). Constraints from the decays $h_2 \to h_1h_1 \to 4f$ (top) and from the decays $\Upsilon \to \gamma h_1 (h_1 \to \mu\mu, \pi\pi, KK)$ (bottom). $\sigma_{4\mu} \equiv \sigma_{h_2}\mathrm{Br}(h_2 \to h_1h_1 \to 4\mu)$. To show the constraint from the $2\mu2\tau$ channel on the same plot we convert it into an effective constraint on $4\mu$ by rescaling it with $\mathrm{Br}(h_1 \to \mu\mu)/\mathrm{Br}(h_1 \to \tau\tau)$ (a model-independent quantity). $\lambda_d$ is a tree-level coupling of the down-type interaction $-(\lambda_d m_{f_d}/\sqrt{2}v)h_1\bar{f}_d f_d$. Light gray and dark gray (blue) points correspond to the gray and dark gray (blue) points in Fig. 3. Purple bands correspond to the points in the scan of Fig. 4.

bosons and $\chi_1$. These facts imply rich Higgs phenomenology in the DLH scenario and can dramatically change the strategies of searching for both the SM-like and the light-Higgs bosons at colliders.)

The Tevatron constraints from the search for $h_2 \to h_1 h_1 \to 4f$ are illustrated in the upper panel of Fig. 2. Almost all points survive. Similar limits from LEP are avoided easily for the present parameter values, because $m_{h_2}$ is above the kinematic threshold [9].

$\Upsilon$ physics constrains models with light states through $\Upsilon \to \gamma(h_1, a_1) \to \gamma(\mu\mu, \pi\pi, KK)$. Figure 2 shows the constraints on the effective coupling $\lambda_d$ of the light state to down-type fermions [10,11]. At tree level, $\lambda_d \approx \frac{v}{\mu} \times (\lambda + \frac{2\varepsilon\mu}{m_Z})$, and the scan points typically approach the constrained region only for $\lambda \gtrsim 0.15$.

$B$ physics may also add nontrivial constraints with a light $a_1$ (e.g., see [8]) or $h_1$, because flavor-violating vertices $b(d, s)(a_1, h_1)$ can be generated at loop level. These vertices, however, depend strongly on the structure of soft breaking parameters (e.g., see [12]). For the input parameters to NMSSMTOOLS used in the scan, the points in the figures are consistent with all $B$-physics constraints including $B_s \to \mu\mu$, $B_d \to X_s\mu\mu$, $b \to s\gamma$, etc.

To study the DM physics in the DLH scenario, we perform a second random scan over its parameter region. Figure 3 shows that the $\chi_1$ DM candidate is characterized by a larger spin-independent direct-detection cross section $\sigma_{\rm SI}$, compared with typical supersymmetric scenarios. For a certain parameter window, the correct relic density and a large $\sigma_{\rm SI}$ consistent with the CoGeNT and DAMA/LIBRA preferred region [13] can be simultaneously achieved, and the scenario remains consistent with current experimental bounds. This has been considered difficult or impossible in supersymmetric models [14].

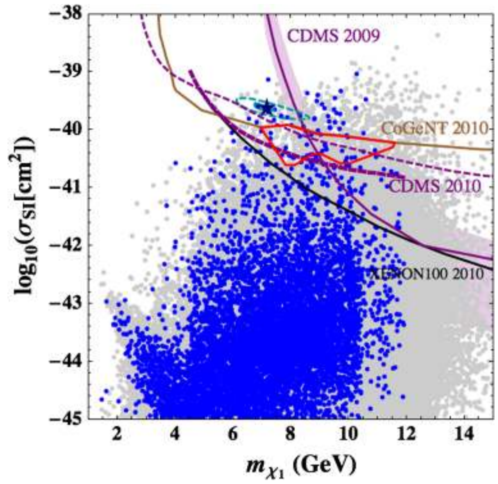


FIG. 3 (color online). Cross section of SI direct detection for $\chi_1$. The scan is over all parameters, in the ranges $0.05 \le \lambda \le 0.15$, $0.001 \le \kappa \le 0.005$, $|\varepsilon'| \le 0.25$, $-40 \le A_\kappa \le 0$ GeV, $5 \le \tan\beta \le 50$ and $100 \le \mu \le 250$ GeV. The dark gray (blue) points have a relic density $0.09 \le \Omega h^2 \le 0.13$. The gray (red) contour is the CoGeNT favored region presented in [16] and the two gray (light blue) dashed circles are the most recent interpretations of fitting CoGeNT + DAMA/LIBRA [13]. All contours assume a local density which may be sensitive to the relic density. The dark gray (purple) dotted and dashed, gray (brown), and black lines are the limits from CDMS [17], CoGeNT [16], and XENON100 [18], respectively. Most CoGeNT favored regions have a tension with the CDMS constraints. Consistency between the CoGeNT preferred regions and the XENON100 constraints can be achieved within the scintillation-efficiency uncertainties of liquid xenon [13].

The large $\sigma_{\rm SI}$ is mainly due to the $h_1$-mediated $t$-channel scattering $\chi_1 q \to \chi_1 q$, and

$$\sigma_{\rm SI} \approx \frac{[(\varepsilon/0.04) + 0.46(\lambda/0.1)(v/\mu)]^2 (y_{h_1\chi_1\chi_1}/0.003)^2 \times 10^{-40}\ \mathrm{cm}^2}{(m_{h_1}/1\ \mathrm{GeV})^4}. \tag{9}$$

The $h_1\chi_1\chi_1$ coupling is reduced to $y_{h_1\chi_1\chi_1} \approx -\sqrt{2}\kappa$ for a singlinolike $\chi_1$ and singletlike $h_1$. The dependence of $\sigma_{\rm SI}$ on $m_{h_1}^{-4}$ is illustrated in the left-hand panels of Fig. 4. For the parameter values given in the caption, the LEP search for $h_2 \to bb$ sets the lower boundary of the contoured region, flavor constraints control the upper-right, vacuum stability sets the upper-left limit, and the upper bound on the relic density controls the left and right limits. The sensitivity to $\tan\beta$ enters mainly via $m_{h_1}$.

The $\chi_1$ relic density is largely controlled by the $a_1$-mediated annihilation $\chi_1\chi_1 \to f\bar{f}$, with cross section

$$\sigma_{f\bar{f}} v_{\chi_1} \approx \frac{3|y_{a_1\chi_1\chi_1} y_{a_1 ff}|^2 (1 - m_f^2/m_{\chi_1}^2)^{1/2}}{32\pi m_{\chi_1}^2 (\delta^2 + |\Gamma_{a_1} m_{a_1}/4m_{\chi_1}^2|^2)}, \tag{10}$$

where $y_{a_1\chi_1\chi_1} \approx -i\sqrt{2}\kappa$ and $\delta \equiv |\frac{1}{1 - v_{\chi_1}^2/4} - \frac{m_{a_1}^2}{4m_{\chi_1}^2}|$, with $v_{\chi_1}$ denoting the relative velocity of the two $\chi_1$'s. $\delta_{v_{\chi_1}\to 0}$ reflects the deviation of $2m_{\chi_1}$ from the $a_1$ resonance. In the typical case $m_{a_1} > 2m_{\chi_1} > 2m_b$, the relic density is

$$\Omega h^2 \approx \frac{0.1(m_{a_1}/15\ \mathrm{GeV})(\Gamma_{a_1}/10^{-5}\ \mathrm{GeV})(0.003/y_{a_1\chi_1\chi_1})^2[(0.1/\lambda)(\mu/v)]^2}{\mathrm{erfc}[(2m_{\chi_1}/m_{a_1})\sqrt{x_f \delta_{v_{\chi_1}\to 0}}]/\mathrm{erfc}(2.2)}, \tag{11}$$

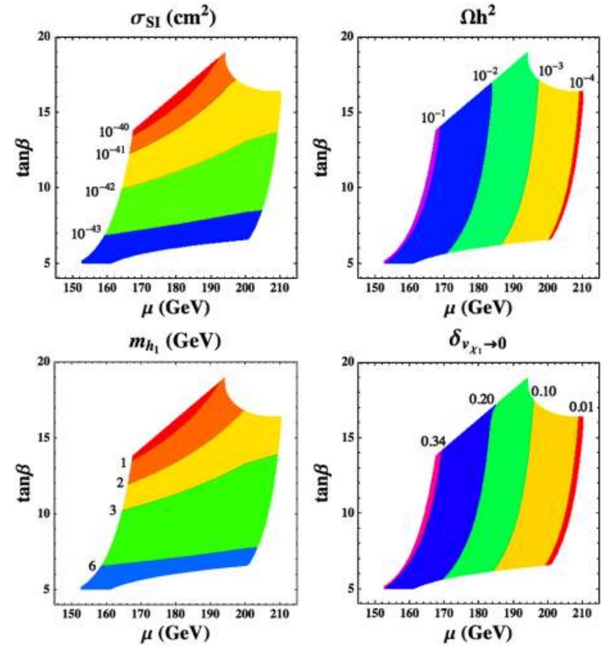


FIG. 4 (color online). Contours of $\sigma_{SI}$ (top left), $\Omega h^2$ (top right), $m_{h_1}$ (left bottom), and $\delta_{v_{\chi_1}\to 0}$ (right bottom) on the $\mu - \tan\beta$ plane, with $\lambda = 0.12$, $\kappa = 2.7 \times 10^{-3}$, $\varepsilon' = 0.15$, and $A_\kappa = -24$ GeV.

where $x_f = m_{\chi_1}/T_f$ is the freeze-out point. As a measure of thermal suppression, $\delta_{v_{\chi_1}\to 0}$ enters the complementary error function obtained from the integral over the Boltzmann distribution. The inverse dependence of $\Omega h^2$ on $\delta_{v_{\chi_1}\to 0}$ is shown in the right-hand panels of Fig. 4. Its sensitivity to $\mu$ is mainly through $\delta_{v_{\chi_1}\to 0}$, as $m_{\chi_1}/m_{a_1} \propto \sqrt{\mu}$ for $\tan\beta \gtrsim 5$. To achieve the correct relic density requires $\delta_{v_{\chi_1}\to 0} \approx 0.30$–$0.35$, which implies $A_\kappa \approx -3.5 m_{\chi_1}$, with a tuning range about $\pm 0.1 m_{\chi_1}$. We emphasize that this process does not generate an antiproton or $\gamma$-ray flux in tension with existing cosmic-ray data because of the Breit-Wigner suppression effect today [15].

Finally, a benchmark point corresponding to the stars in Figs. 2 and 3 is given in Table I. Changing the sfermion or gaugino parameters can change the details of the phenomenology, but the basic features will remain intact. We reserve a further analysis of this scenario for future work.

Work at ANL is supported in part by the U.S. DOE Grant No. DE-AC02-06CH11357. Work at EFI is supported in part by the DOE Grant No. DE-FG02-90ER40560. T. L. is supported by a Fermi-McCormick grant and the DOE Grant No. DE-FG02-91ER40618 at University of California, Santa Barbara. L.-T. W. is supported by the NSF under Grant No. PHY-0756966 and the DOE OJI under Grant No. DE-FG02-90ER40542. H. Z. is supported by the National NSF of China under Grant No. 10975004 and the CSC File No. 2009601282.

TABLE I. Benchmark point. We use the units cm$^2$ for $\sigma_{SI}$ and GeV for dimensionful input parameters, and denote Br($h_2 \to h_1 h_1$) as Brhh and Br($h_2 \to a_1 a_1$) as Braa. Soft sfermion and gaugino parameters are as given in the caption of Fig. 1.

| $\lambda$ | $\kappa(10^{-3})$ | $A_\lambda(10^3)$ | $A_\kappa$ | $\mu$ | $\tan\beta$ | $m_{h_1}$ |
|---|---|---|---|---|---|---|
| 0.1205 | 2.720 | 2.661 | −24.03 | 168.0 | 13.77 | 0.811 |
| $m_{a_1}$ | $m_{\chi_1}$ | $m_{h_2}$ | Brhh | Braa | $\Omega h^2$ | $\sigma_{SI}$ $(10^{-40})$ |
| 16.7 | 7.20 | 116 | 0.158% | 0.310% | 0.112 | 2.34 |


[1] B. A. Dobrescu *et al.*, Phys. Rev. D **63**, 075003 (2001).

[2] R. Dermisek *et al.*, Phys. Rev. Lett. **95**, 041801 (2005).

[3] P. Ciafaloni *et al.*, Phys. Lett. B **404**, 83 (1997); D. J. Miller *et al.*, arXiv:hep-ph/0501139.

[4] S. Schael *et al.* (ALEPH, DELPHI, L3, and OPAL Collaborations), Eur. Phys. J. C **47**, 547 (2006); S. Schael *et al.* (ALEPH Collaboration), J. High Energy Phys. 05 (2010) 049.

[5] V. M. Abazov *et al.* (D0 Collaboration), Phys. Rev. Lett. **103**, 061801 (2009).

[6] U. Ellwanger *et al.*, J. High Energy Phys. 02 (2005) 066.

[7] G. Belanger *et al.*, Comput. Phys. Commun. **182**, 842 (2011).

[8] U. Ellwanger *et al.*, Phys. Rep. **496**, 1 (2010).

[9] The LEP and Tevatron constraints from the channel $h_2 \to a_1 a_1$ are included in NMSSMTOOLS and in our code, respectively. Points are omitted if the limit is violated. Similarly, the constraint from $\Upsilon \to \gamma a_1$ is checked by NMSSMTOOLS, so we present only the limit from $\Upsilon \to \gamma h_1$ in Fig. 2. For the numerical results presented in this Letter we incorporate *all* built-in checks in NMSSMTOOLS 2.3.1 (including those from LEP Higgs searches, superpartner searches, $g_\mu - 2$, flavor physics, $Z$ decay, $\eta_b$ physics, etc.), except the DM relic density. The difference between Fig. 1 and Figs. 3 and 4 is that, in the latter, $\Omega h^2 \leq 0.13$ is also required.

[10] D. McKeen, Phys. Rev. D **79**, 114001 (2009); Phys. Rev. D **79**, 015007 (2009).

[11] B. Aubert *et al.* (BABAR Collaboration), Phys. Rev. Lett. **103**, 081803 (2009).

[12] M. Carena *et al.*, Phys. Rev. D **79**, 075025 (2009).

[13] D. Hooper *et al.*, Phys. Rev. D **82**, 123509 (2010).

[14] D. Feldman *et al.*, Phys. Rev. D **81**, 117701 (2010); E. Kuflik *et al.*, Phys. Rev. D **81**, 111701 (2010); K. J. Bae *et al.*, Phys. Rev. D **82**, 115014 (2010); J. Cao *et al.*, J. High Energy Phys. 07 (2010) 044; D. Das *et al.*, J. High Energy Phys. 09 (2010) 085; A. Bottino *et al.*, Phys. Rev. D **67**, 063519 (2003); A. V. Belikov *et al.*, arXiv:1009.0549; J. F. Gunion *et al.*, arXiv:1009.2555.

[15] O. Adriani *et al.* (PAMELA Collaboration), Phys. Rev. Lett. **105**, 121101 (2010); M. Ackermann *et al.* (Fermi LAT Collaboration), Phys. Rev. D **82**, 092004 (2010); J. Lavalle, Phys. Rev. D **82**, 081302 (2010).

[16] C. E. Aalseth *et al.* (CoGeNT Collaboration), arXiv:1002.4703 [Phys. Rev Lett. (to be published)].

[17] Z. Ahmed *et al.* (CDMS-II Collaboration), Science **327**, 1619 (2010); D. Akerib *et al.* (CDMS Collaboration), Phys. Rev. D **82**, 122004 (2010); Z. Ahmed *et al.* (CDMS-II Collaboration), arXiv:1011.2482.

[18] E. Aprile *et al.* (XENON100 Collaboration), arXiv:1005.0380.